

Technology Development for Exoplanet Missions

Technology Milestone Whitepaper

Laboratory Demonstration of High Contrast Using PIAACMC on a Segmented Aperture

Ruslan Belikov (PI), Eduardo Bendek (deputy PI), Dan Sirbu, Eugene Pluzhnik, Stephen Bryson
(NASA Ames Research Center)

Brian Kern (Institutional PI), David Marx, Dan Wilson
(NASA Jet Propulsion Laboratory)

Olivier Guyon, Justin Knight
(The University of Arizona)

February 6, 2018

Approvals

Released by

Ruslan Belikov
Principal Investigator, NASA ARC

Date

Approved by

Nicholas Siegler
Exoplanet Exploration Program Chief Technologist, NASA JPL

Date

Brendan Crill
Exoplanet Exploration Program Deputy Chief Technologist, NASA JPL

Date

Douglas Hudgins
Exoplanet Exploration Program Scientist, NASA-HQ

Date

Contents

Contents.....	2
1 Objective	3
2 Introduction / Background	3
2.1 PIAACMC motivation and significance.....	3
2.1.1 Science significance.....	3
2.1.2 Significance to other coronagraph architectures	4
2.2 PIAACMC theory.....	4
2.2.1 PIAACMC concept and reason for compatibility with segmented apertures....	4
2.2.2 Comparison of segmentation compatibility with other designs	5
3 Milestones Definition.....	7
4 Experiment Description	7
4.1 PIAACMC design tools and theoretical performance	8
4.1.1 Ideal PIAACMC design and performance	8
4.1.2 Manufacturable PIAACMC designs.....	8
4.1.3 Aberrations specific to segmented telescopes.....	9
4.2 PIAACMC fabrication.....	10
4.2.1 PIAA Mirror fabrication	10
4.2.2 CMC Mask fabrication	10
4.2.3 Other components.....	12
4.3 Performance Modeling.....	12
4.4 System Testing	13
4.4.1 Description of HCIT-2 and past performance with PIAA and PIAACMC	13
4.4.2 HCIT-2 proposed testing.....	13
4.4.3 ACE testing	15
5 Data Measurement & Analysis.....	16
5.1 Definitions.....	16
5.1.1 “Raw” Image and “Calibrated” Image (milestones 2 and 3 only).....	17
5.1.2 DM flat (milestones 2 and 3 only).....	17
5.1.3 Star (milestones 2 and 3 only).....	17
5.1.4 Wavefront control iteration.	17
5.1.5 Contrast field.....	17
5.1.6 Contrast value.....	17
5.1.7 “Statistical Confidence” (milestones 2 and 3 only).....	18
5.2 Measurement of the Star Brightness (milestones 2 and 3 only).....	18
5.3 Measurement of the focal plane scale.....	19
5.4 Measurement of the Coronagraph Contrast Field.....	19
5.5 Contrast value for a single measurement	20
5.6 Milestone Verification Demonstration Procedure.....	20
5.7 Milestone Certification Data Package	21
6 Success Criteria	21
7 Schedule	22
8 References and Citations.....	24
9 List of Acronyms.....	26

1 Objective

The objective of this effort is to demonstrate and mature starlight suppression technology with the Phase Induced Amplitude Apodization Complex Mask Coronagraph (PIAACMC, Guyon et al. 2014c) for segmented apertures. Specifically, we plan to perform a laboratory demonstration in vacuum of 10^{-9} contrast with an inner working angle of $2 \lambda/D$ (or better) in a 10% bandpass centered at 650 nm, using segmented apertures representative of those expected for the LUVOIR and HabEx missions (if segmented). This is the basis of the final milestone of our effort, described in more detail in section 3.

2 Introduction / Background

2.1 PIAACMC motivation and significance

PIAACMC (Phase-Induced Amplitude Apodization Complex Mask Coronagraph) is a high performance coronagraph capable of approaching fundamental limits for any theoretically possible coronagraph architecture. It has on the order of 100% coronagraphic throughput, and inner working angles (IWAs) that can go as low as $0.5 \lambda/D$. Its sensitivity to tip/tilt aberrations is close to theoretically best for any chosen inner working angle (at least for aggressive inner working angles), and can be traded against inner working angle (Guyon et al. 2014c). Thus, the PIAACMC represents a path to reach physics-limited (rather than coronagraph-architecture-limited) starlight suppression performance for a given aperture and stability environment. This path can enable taking full advantage of the large apertures on future telescopes like LUVOIR and HabEx, and maximize their science and cost effectiveness. The work proposed here is a significant step along that path (as would be the advancement of any other architecture that approaches theoretically optimal performance, such as the vector vortex coronagraph, with which PIAA nicely hybridizes for segmented apertures).

In certain key respects, the performance gains enabled by high performance coronagraphs are equivalent to increasing the aperture of the telescope. For example, a PIAACMC coronagraph with 80% throughput and an inner working angle of $1.5 \lambda/D$ on an 4m aperture is equivalent to an 8m telescope that has a coronagraph with a 20% throughput and $3 \lambda/D$ (similar to some of the designs of, for example, the band-limited Lyot or the Shaped Pupil Coronagraphs), in terms of photon flux and inner working angle in units of arcseconds. Conversely, missions can save significant costs by reducing the aperture and improving coronagraph performance, leaving the science yield unchanged.

2.1.1 Science significance

The importance of enabling small IWAs is highlighted in Stark et al. (2015). In this study, the mission yield of Earth-like exoplanets in the habitable zones of their stars grew approximately inversely to IWA, meaning a mission with half the IWA doubles the yield of Earth-like exoplanets. Considering all exoplanets (not just Earth-like exoplanets), the yield grows as the inverse 3rd power of IWA for a target-limited mission. Thus, advancing coronagraph architectures with small IWAs has a greater impact on expected yield than parameters such as increasing throughput or improving contrast.

A throughput improvement also increases yield via several ways. It leads to faster wavefront control loops (at least if the loop rate is photon-noise limited) and thus better correction of dynamic

speckles, improving raw contrast. Higher photon fluxes also enable better post-processing (in the photon-noise limited regime), enabling deeper post-processed contrasts. Higher SNR and/or higher spectral resolution are enabled by higher throughput. For time-limited missions, throughput leads directly to higher yield even if nothing else is improved.

A laboratory demonstration of PIAACMC is valuable for the community because it validates the combination of small IWA and high throughput that maximizes science return for a given aperture.

2.1.2 Significance to other coronagraph architectures

In addition to being a stand-alone architecture, PIAACMC can be hybridized with other coronagraph architectures, which is sometimes necessary to make those architectures compatible with segmented apertures. For example, the Vortex coronagraph requires an apodization for segmented apertures, which can be implemented by a set of PIAA mirrors. Similarly, the apodization in the Apodized Pupil Lyot Coronagraph (APLC) can be implemented using PIAA mirrors, which improves throughput and inner working angle. The CMC mask (design tools as well as fabrication methods) developed as part of this project may also be useful as an alternative mask for the Bandlimited Lyot and related coronagraphs. It may also be productive to explore the possibility of enhancing the mask in the Vortex coronagraph with CMC-like features, which may help with segmented apertures.

More generally, in the near future, it may no longer be meaningful to think in terms of different coronagraph architectures, but rather as a collection of synergistic technologies that can be combined to optimize a coronagraph within a rich design space that is now shared by different classic architectures. In addition to the objective demonstration of starlight suppression performance, this work represents an advancement of PIAA and CMC technologies for the benefit of other classic architectures in this shared coronagraph design space, in particular the benefits to the Vortex and APLC coronagraphs as described above.

2.2 PIAACMC theory

2.2.1 PIAACMC concept and reason for compatibility with segmented apertures

Compared to unobscured apertures, segmented apertures may or may not present increased challenges for high contrast coronagraphic performance, depending on the coronagraph architecture. N'Diaye et al. (2016) present an overview of different coronagraph architectures and their approaches to dealing with segmented apertures. Investigators included in this proposal are participating in Stuart Shakan's ExEP-funded effort to develop and evaluate specific designs for coronagraphs on segmented apertures with different coronagraph architectures, the Segmented Coronagraph Design & Analysis task (SCDA, http://exep.jpl.nasa.gov/files/exep/SCDA_Summary.pdf).

In this section we go over the basics of PIAACMC theory and show why it is naturally compatible with segmented apertures. The PIAACMC coronagraph is diagrammed in Figure 1 and consists of:

- A pair of PIAA mirrors that remap the intensity profile of the incoming beam (P) from a top-hat shape into a specially designed apodization (A). For unobstructed apertures, this apodization has a so-called prolate-spheroidal shape, but for obstructed apertures it becomes more complicated and needs to be numerically optimized.

- A phase-shifting partially transmissive focal plane mask. A π -phase-shifting mask can cause complete destructive interference of light in the openings of the Lyot stop, if its transmission is chosen appropriately. The "ideal" π -phase-shifting partially transmitting mask (over an entire wavelength bandpass) is challenging to manufacture directly, so practical PIAACMC designs use an array of fully reflective (or fully transmissive) zones, each with some specific height to generate some desired optical path difference for that zone. The zone heights are optimized to achieve the best contrast in a desired region of interest. CMC masks do not absorb light, rather they redirect on-axis starlight to the Lyot stop.
- A Lyot stop blocks starlight that is diffracted by the focal plane mask. In a simplistic treatment, the Lyot stop will be identical to the (remapped) segmented pupil obscuration, as shown in Figure 1. In practice, more area is blocked to accommodate real-world near-field diffraction and other practical concerns.
- An (optional) inverse PIAA optics is used to undo the pupil remapping, without which the field of view is limited by off-axis distortions caused by the PIAA optics. For many practical designs, including the WFIRST PIAACMC design, this is not necessary.

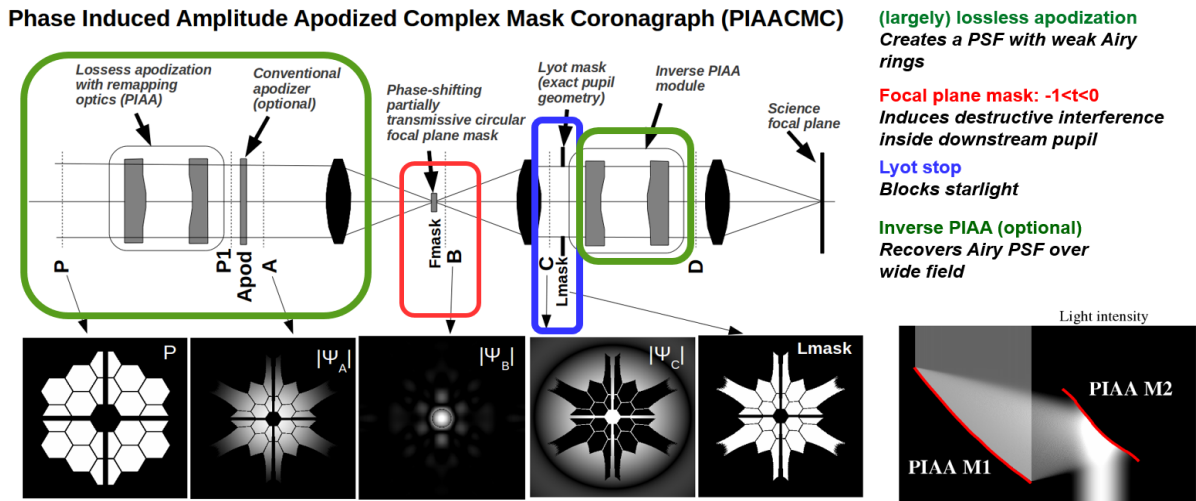


Figure 1. Schematic diagram of PIAACMC coronagraph.

2.2.2 Comparison of segmentation compatibility with other designs

Figure 2 compares PIAACMC's theoretical compatibility with segmented apertures with other architectures. Two different cases are shown: one for a band-limited style of coronagraph intended to operate on a uniformly illuminated aperture, and one for a PIAACMC that creates an apodized pupil. In each case, the focal plane mask produces a Lyot-plane E -field that is the convolution of the pupil E -field and the Fourier transform of the focal plane mask transmission, which is then filtered by the Lyot stop. In Fig. 2, the pupil E -field is represented in blue, the on-axis E -field diffracted by the focal plane mask is shown in green, and the resulting E -field in the Lyot plane is shown in red. The Lyot stop is typically sized to block the region of nonzero E -field for an on-axis source (the star), but left as open as possible to maximize the throughput of planet (off-axis) light. The open area of the Lyot stop is shown as a hatched region in Fig. 2.

The diffractive challenges posed by segmented apertures can be abstracted by identifying the characteristic size of contiguous regions of the pupil. For an unobscured pupil, the entire pupil is a single contiguous region, of size D . For the segmented pupil in Fig. 2, each segment is a contiguous region of size $D/7$. In each case, the Lyot-plane E -field spreading effect of a focal plane mask designed for a particular IWA scales as IWA^{-1} (as a Fourier transform). As can be seen graphically, for the band-limited coronagraph to maintain the same throughput on a segmented aperture (with 7 segments across D , see Fig. 2) as the equivalent unobscured aperture, the band-limited focal plane mask IWA would have to grow by a factor of 7 (e.g., from $3 \lambda/D$ to $21 \lambda/D$ IWA), a clearly irrelevant coronagraph design.

The SCDA task will explore the appropriate questions of how an un-apodized Lyot-style coronagraph will perform on a segmented aperture, where contiguous zones may span only $D/7$, more than a factor of 2 more challenging than WFIRST.

With the freedom to define the apodization of the pupil as well as the design of the focal plane mask, apodized coronagraph designs can accomplish full extinction of on-axis starlight without decreasing the size of the Lyot stop relative to the input pupil. This is true for segmented, obscured, and unobscured apertures. Comparing classical apodization (absorption) to PIAA, the throughput differs by approximately a factor of 2 for small-IWA designs (Guyon et al. 2014c), with PIAA being essentially lossless, coronagraphically speaking.

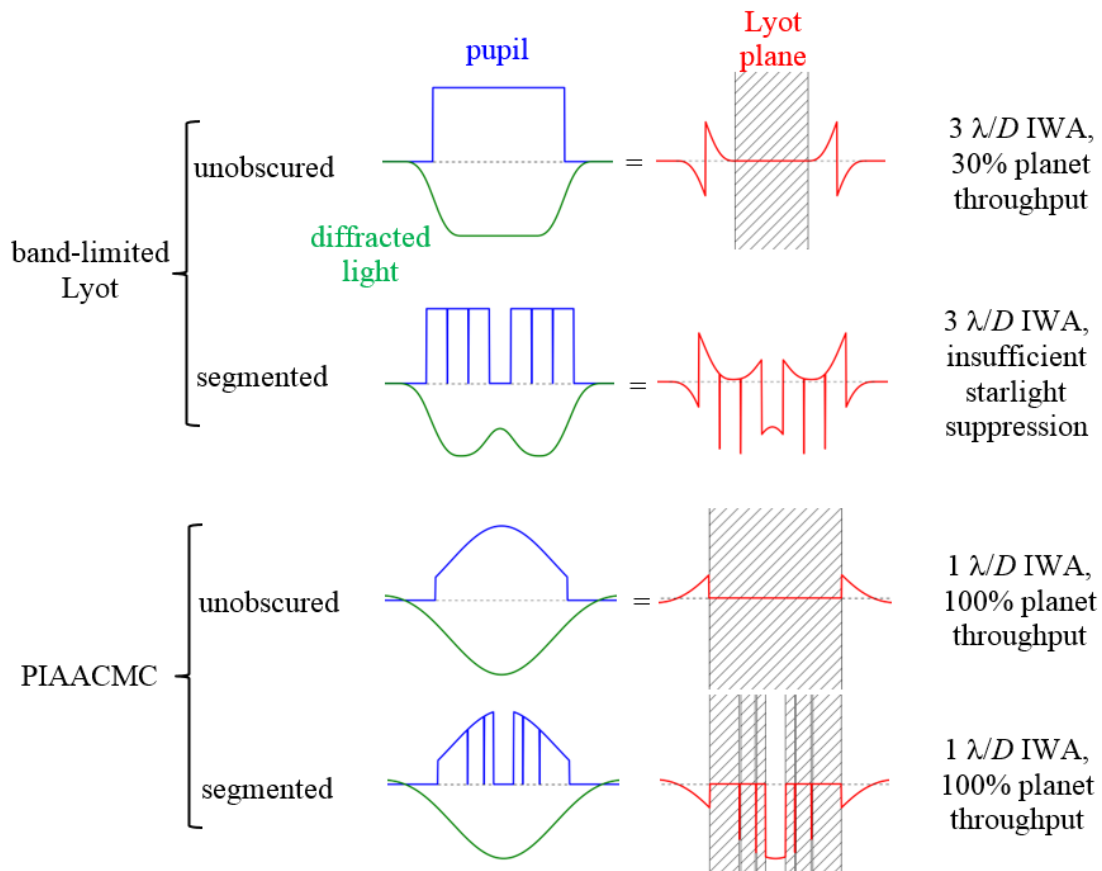


Figure 2. Comparison of diffractive effect of segmented apertures relative to unobscured apertures, for a $3 \lambda/D$ IWA band-limited Lyot and a $1 \lambda/D$ IWA PIAACMC architecture. In each row, the blue line is a 1D slice of E -field amplitude in the pupil, the green line is the E -field diffracted from an on-axis point source by the focal plane mask, and the red line is the Lyot-plane E -field (blue + green = red). The hatched region is transmitted by the Lyot stop, which determines the planet throughput. The segmented band-limited Lyot coronagraph does not produce any Lyot area free of on-axis starlight.

3 Milestones Definition

***Milestone 1** (July 13, 2018). Demonstration of an end-to-end computer simulation of proposed HCIT-2 layouts, with the new PIAACMC design and wavefront control, that reaches the following performance: $1e-9$ raw contrast averaged between 2 and $8 \lambda/D$, under the following conditions:*

- (a) in a 10% wavelength band (baseline center wavelength 650nm);*
- (b) in one polarization (polarized source and analyzer in front of science focal plane);*
- (c) for the version of the LUVOIR pupil as specified by STDT as of Dec 2017;*
- (d) tip/tilt jitter of $0.004 \lambda/D$ rms per axis.*

***Milestone 2.** (Dec 10, 2019) Laboratory demonstration of $1e-9$ raw contrast averaged between 2 and $8 \lambda/D$, under the following conditions:*

- (a) in monochromatic light (baseline wavelength 650nm);*
- (b) in one polarization (polarized source and analyzer in front of science focal plane);*
- (c) for the version of the LUVOIR pupil as specified by STDT as of Dec 2017;*
- (d) assuming that level of tip/tilt error on HCIT is $< 0.004 \lambda/D$ rms per axis. This level of error will either be confirmed in year one, or milestone will be rewritten to correspond to actual testbed jitter.*

***Milestone 3.** (Dec 18, 2020) Same as milestone 2, but in broadband light. Specifically, laboratory demonstration of $1e-9$ raw contrast averaged between 2 and $8 \lambda/D$, under the following conditions:*

- (a) in a 10% wavelength band (baseline center wavelength 650nm);*
- (b) in one polarization (polarized source and analyzer in front of science focal plane);*
- (c) for the version of the LUVOIR pupil as specified by STDT as of Dec 2017;*
- (d) assuming that level of tip/tilt error on HCIT is $< 0.004 \lambda/D$ rms per axis. This level of error will either be confirmed in year one, or milestone will be rewritten to correspond to actual testbed jitter.*

Notes:

- As described in section 4.1.2.1, we expect the jitter on HCIT-2 to be $0.002 \lambda/D$ (rms per axis), and are designing our coronagraph to be tolerant to $0.008 \lambda/D$ in order to have sufficient margin on both sides of the $0.004 \lambda/D$ figure in part (d) of each milestone. Thus, the chances of 2(d) and 3(d) being wrong are small. Nevertheless, they do pose a risk. To mitigate this risk, we will plan to measure the testbed jitter early, as part of our testbed preparation activities in year 1 as well as during the first vacuum tests (see Section 5). Should the testbed jitter still prove too high, the easiest way to accommodate it is to change the IWA of the design in subsequent mask iterations and do a minor IWA adjustment in the milestones. Theoretically, jitter sensitivity is a very strong function of IWA: a 10x worse jitter can be accommodated by increasing the IWA from $1.9 \lambda/D$ to $2.2 \lambda/D$ (Guyon et al. 2010).
- Polarization (parts (b) in each milestone) will of course incur a 50% throughput hit. To avoid this on a real instrument, a system can be designed that has less polarization-dependent error, or two independent coronagraphs can be made for each polarization. It is also possible that our system will have negligible polarization-dependent error, thus allowing us to reach the milestones without any throughput reducing polarizers, which we will attempt as a stretch goal. However, the milestones will be considered successful if they are met at least with a polarizer.

4 Experiment Description

4.1 PIAACMC design tools and theoretical performance

4.1.1 Ideal PIAACMC design and performance

The ideal PIAACMC design, i.e. one with an ideal CMC mask, is relatively trivial to design for any aperture (Guyon et al. 2014c), and is the first step in designing a manufacturable PIAACMC design. Ideal PIAACMC has possibly the highest throughput and smallest IWA of published designs (ideal or not) for segmented apertures. As shown in Figure 3, these designs have $> 99\%$ nominal coronagraphic transmission combined with IWAs below $1 \lambda/D$. The performance calculated in Guyon et al. 2014c is overly simplistic, by not including plane-to-plane propagation effects (near-field Fresnel diffraction between PIAA mirrors) or finite bandwidths. These designs also were not optimized to reduce tip-tilt sensitivity. The designs from Guyon et al. 2014c are summarized in Fig.3, shown alongside the pupils they were computed for, ranging from obscured (Subaru) to finely segmented (E-ELT). Note that in Fig. 3, the PIAACMC designs for obscured (Subaru) and segmented (all others) apertures produce similar throughputs.



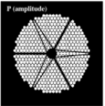
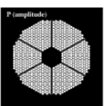
	Design	Throughput	IWA
	Subaru Telescope pupil		
	Subaru PIAACMC #1	99.91%	0.67 λ/D
	Subaru PIAACMC #2	99.39%	0.88 λ/D
	Subaru PIAACMC #3	97.04%	1.11 λ/D
	Giant Magellan Telescope (GMT) pupil		
	GMT PIAACMC #1	99.98%	0.72 λ/D
	GMT PIAACMC #2	99.47%	0.89 λ/D
	GMT PIAACMC #3	99.14%	0.92 λ/D
	Thirty Meter Telescope (TMT) pupil		
	TMT PIAACMC #1	99.80%	0.78 λ/D
	TMT PIAACMC #2	98.51%	0.94 λ/D
	TMT PIAACMC #3	98.71%	0.99 λ/D
	European Extremely Large Telescope (E-ELT)		
	E-ELT PIAACMC #1	97.77%	0.81 λ/D
	E-ELT PIAACMC #2	99.50%	0.93 λ/D
	E-ELT PIAACMC #3	99.42%	0.98 λ/D

Figure 3. Table of PIAACMC designs on obscured and segmented apertures, from Guyon et al. (2014c). Images are pupil input into each design. Note that throughput numbers are all high, whether on obscured (Subaru) or finely segmented (E-ELT) apertures. The pupils on the left correspond to (top to bottom): Subaru, GMT, TMT, and E-ELT. PIAACMC 1, 2, and 3 correspond to designs with different inner working angles (IWAs), an adjustable parameter.

4.1.2 Manufacturable PIAACMC designs

Technology does not yet exist to manufacture an ideal CMC mask (i.e. a disk with an achromatic pi phase shift), but fortunately a technique exists to recover much of its effective functionality with a fully reflective or transmissive holographic phase mask, i.e. one with a variable optical path difference as a function of position.

In order to design a manufacturable PIAACMC mask, an optimization code is used, originally developed by Guyon and is currently being developed further by Bryson. The algorithm first creates an ideal PIAACMC design (per Guyon 2014c) and uses it as a starting point for further optimizations. Number of zones and their shapes are defined, as well as the number and locations

of the Lyot stops. The algorithm then performs several iterations of optimizing the heights of the CMC mask zones, slight alterations of the original PIAA optics shapes, and the Lyot stop(s). Included in the algorithm is the ability to optimize the sensitivity to low-order aberrations. An example of the output of this algorithm for a segmented aperture, likely very similar to the design that will be used by this effort, has a 70% throughput, $1 \lambda/D$ inner working angle, Lyot stop, and no inverse PIAA.

4.1.2.1 Sensitivity to aberrations and polarization

PIAACMC designs have known sensitivity to low order aberrations and polarization, which is largely a consequence of their aggressive IWAs. The sensitivity to tip/tilt aberrations for ideal PIAACMC designs improves steadily as IWA is made larger (Guyon et al. 2010), and has a very similar sensitivity to the vector vortex coronagraph when both are designed to have the same IWA. Furthermore, both PIAACMC and the vortex coronagraphs appear to be close to fundamental limits for tip/tilt sensitivity, constrained by their IWA alone. There is an open question about whether PIAACMC can be made as insensitive to low order aberrations as, say, the shaped pupil coronagraph, if both coronagraphs were designed for an IWA typical of the SPC (i.e. $\sim 3 \lambda/D$). Although this part of PIAACMC design space has been poorly explored, there is currently no reason to believe that a properly optimized PIAACMC design will be more sensitive to aberrations than any other coronagraph, when both are designed for the same IWA.

All realistic space mission designs experience polarization-specific aberrations through the variation of angles of incidence across powered optics (nearly universally dominated by the telescope primary mirror). In a coronagraphic performance context, these aberrations predominately appear as astigmatism and tip-tilt phase aberrations. As with tip-tilt, astigmatism sensitivity is higher for smaller IWA coronagraphs. In particular, models of the WFIRST PIAACMC design showed a significant effect due to polarization-induced aberrations, again largely a consequence of the $1.3 \lambda/D$ IWA (aggressively small) WFIRST PIAACMC design. This also suggests that it is reasonable to expect that designing a PIAACMC coronagraph that has a larger IWA will make it as insensitive to polarization-induced aberrations as any other architecture with that IWA (provided that tolerance to low-order aberrations is part of the optimization goal).

The performance levels selected for the milestones, and in particular, the amount of jitter we expect to tolerate, are based in part on Guyon et al. 2010 as well as the measured sensitivities of the WFIRST PIAACMC tests (WFIRST milestone 3 report), which are consistent with each other. In particular, for a PIAACMC coronagraph with an inner working angle of $1.9 \lambda/D$, the effect of $0.004 \lambda/D$ jitter is theoretically expected to be $2e-10$ contrast. As part of this work, we will explore the trade space of IWA and sensitivity to low-order aberrations further, and select a design that has the most aggressive IWA while maintaining the sensitivity to aberrations compatible with good performance on HabEx and LUVOIR. We will also compare the theoretical sensitivity to different levels of tip/tilt and defocus errors against actual lab measurements.

4.1.3 Aberrations specific to segmented telescopes

This effort will not design for, or directly test aberrations specific to segmented pupils, apart from the fundamental amplitude pattern particular to the segment gaps. Segmented apertures are expected to carry specific phase effects distinct from monolithic apertures, such as edge roll-off and dynamic segment piston motions. These effects pose challenges to all coronagraph architectures, largely due to the fact that in the pupil, their spatial frequency components are indistinguishable from the spatial frequency components corresponding to the off-axis planet light

that the coronagraph must pass. The mitigation strategies for dynamic segment piston motions, for example, are likely to be addressed in a coronagraph-independent manner. This proposed effort will not simultaneously address the architecture-specific question of PIAACMC operation on a static segmented aperture and the architecture-independent question of segment piston error control.

Independent of this effort, HCIT may invest in a high-fidelity segmented pupil simulator, but that is not offered for general future use at this time.

4.2 PIAACMC fabrication

4.2.1 PIAA Mirror fabrication

We will take an approach to mirror fabrication very similar to that used by the WFIRST PIAACMC experiment (Kern et al. 2016). The WFIRST PIAACMC modeling showed that the tolerance for PIAA mirror surface errors was relatively loose, allowing 20 nm rms surface errors per optic without appreciable loss of performance. This level of surface error, for azimuthally symmetric shapes at the size of the PIAA mirrors (~ 2 inch and 0.5 inch diameter) was reliably achieved from standard diamond turning of aluminum substrates (WFIRST PIAA mirrors achieved 15 and 12 nm rms surface errors), with a short lead time (12 weeks). We will repeat the same process, procuring diamond-turned aluminum mirrors arranged in an on-axis telescope assembly. Testing of the mirrors individually requires computer generated holograms (CGHs) to allow a null-test of the desired surfaces, and again in this context we will repeat the experience of the WFIRST experiment, specifying and procuring CGHs specific to the PIAA mirror shapes once the design is finalized.

4.2.2 CMC Mask fabrication

4.2.2.1 Baseline CMC Mask

The WFIRST PIAACMC experiment, now concluded, fabricated PIAACMC occulting masks at JPL’s MDL (MicroDevices Laboratory) facilities, and included a detailed characterization analysis that was summarized in the WFIRST CGI Milestone #3 (successfully completed in Dec. 2014). The analysis of those characterization data identified the mask surface height errors as relevant for coronagraph performance at the $\sim 10^{-8}$ level. Similar masks were then fabricated and tested for the WFIRST CGI Milestone #8 (see Fig. 4), achieving $\sim 10^{-8}$ contrast in 10% broadband light, as well as one alternative fabrication method explored (Newman et al. 2015).

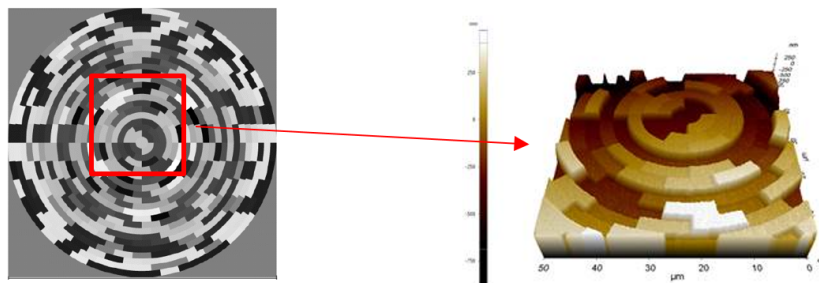


Figure 4. (Left) Design e-beam lithography depths of WFIRST “Gen 3” focal plane mask. (Right) atomic force microscope height measurements of fabricated WFIRST focal plane mask. The mask is uniformly reflective, 155 μm in diameter, with peak-to-valley height 0.6 μm .

WFIRST concluded the PIAACMC experiment before the analysis had positively identified the factors that ultimately limited performance. The two leading candidates were the occulting mask surface height errors and the wavefront control algorithm application.

As part of this effort, we will fabricate, characterize, and coronagraphically test PIAACMC occulting masks made at JPL’s MDL, using similar techniques to those used by WFIRST. We will perform several iterations of mask design, with information about fabrication errors in earlier masks feeding into better calibration of the next iteration.

Because of the possibility that performance will be limited by the mask fabrication errors, special attention will be paid to the feedback of characterization and performance data into the fabrication process itself, in an iterative process. In detail, there will be four cycles of MDL mask fabrication, each cycle incorporating two iterations of mask fabrication and characterization. These will be interleaved with coronagraphic testing and possible design updates, allowing all relevant inputs to be factored into the succeeding cycle of fabrication and characterization.

4.2.2.2 Alternative CMC mask

We are baselining the MDL CMC mask from the previous subsection because we have had past successes with it (WFIRST milestone 3 report, 2015). However, in addition to the baseline mask, we also have a parallel track to explore an alternative CMC mask design and fabrication at UofA by Co-Is Guyon and Knight. This has several benefits: (a) the focal plane mask is the single most challenging part of the PIAACMC fabrication, so having an alternative parallel track is essential to mitigate risk; (b) the UofA mask can potentially be produced with smaller errors than the MDL mask; (c) it is possible to make transmissive masks (as opposed to the reflective MDL CMC masks), and increase the available options for the instrument layout; (d) the UofA approach can be applied to other coronagraphs, such as the APLC and possibly the Vortex coronagraph; (e) continued exploration and development of masks is necessary to improve sensitivity to polarization and stellar sizes, and efficiently redirecting starlight to the LOWFS.

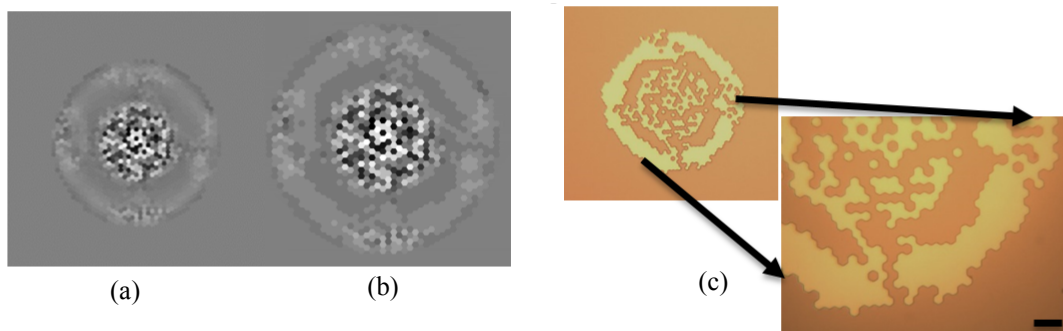


Figure 5. (a) The ideal phase PIAACMC focal plane mask designed for the Subaru telescope SCExAO bench. (b) The discretized mask design for fabrication contains sixteen distinct levels. (c) The first photoresist exposure pattern.

This mask is to be tested with the coronagraph at ARC until it is mature enough to be put in vacuum at HCIT. Depending on the performance of both MDL and UofA masks, we will have several decision points about which mask to test in vacuum.

The fabrication efforts already underway, funded internally at University of Arizona through spring 2017, focus on photolithographic production of a PIAACMC FPM designed for the use in the SCExAO system at the Subaru telescope. This is accomplished with an approximately 300 micron diameter FPM consisting of a tiling of 1237 hexagons which are allowed to cover a range

of continuous depths in an ideal PIAACMC design (Knight et al. 2017). The ideal FPM is shown in Figure 5(a,b) with each regular hexagon having 4.55 micron edges.

In general, mature photolithographic and etching processes work on the principle of binary optics, meaning achievable depths are discrete and scale as 2^n , where n is the number of etch steps. The principal fabrication technique being explored at UofA is a combination of binary photolithographic and etching processes intended to approximate an ideal PIAACMC FPM design as closely as available tooling and techniques allow. Figure 5(c) demonstrates the photoresist pattern of the first exposure of an existing design.

Although specific manufacturing sensitivities will depend on the final design chosen for the LUVOIR/HabEx segmented apertures, previous PIAACMC mask manufacturing errors were split along three main categories: (1) segment height errors, (2) wide-angle surrounding features, and (3) sharpness of segment transitions (Kern et al. 2016). The WFIRST PIAACMC masks were limited by the electron-beam process' physical extent resulting in wide-angle surrounding artifacts. A new e-beam machine is expected to be used for masks manufactured by MDL for this project which is expected to relax this limit by a factor of 2. The lithographic process at UofA, however, is expected to not have this limitation at all. Additionally, the alternative process may allow using a different design space -- for example, the preliminary UofA masks shown in Figure 5(c) use a different hexagonal segment geometry -- as well as designing for robustness to identified experimental limitations. Finally, characterization of manufactured masks such as AFM measurements would allow using a more accurate empirical model of the mask to be used by EFC, as well as being able to select the best mask out of the ones manufactured based on predictions of EFC.

4.2.3 Other components

In addition to the PIAA mirrors and CMC occulting masks, the pupil obscuration, Lyot stop, and field stops will be fabricated. These can be done inexpensively with laser cutting of foil (for example), and are low-risk, low-cost options.

The segmentation of the input pupil will be represented in this experiment only as an opaque mask (transmission through cutouts in foil), creating “segment gaps”.

4.3 Performance Modeling

To model the performance of the system, we will use two independent and mature PIAA propagation and wavefront control libraries based on the Electric Field Conjugation (Give'on et al. 2007) algorithm: one at JPL and one at ARC. The JPL library was used to model the performance of the WFIRST PIAACMC at JPL, and has been validated both on PIAACMC WFIRST demonstrations as well as against PROPER (Krist et al. 2014, Krist et al. 2015). NASA ARC has an independent library that has been validated on ACE coronagraphic demonstrations. We will advance the understanding / validation of the two codes on lab data. Specifically, modeling efforts will be carried in parallel and compared against laboratory tests at HCIT-2 and ACE testbeds, with masks made by MDL and UofA. Laboratory results will be fed back into the models to recalibrate them and modeling results will be used to predict and inform the next iteration of laboratory tests. We plan to use the ACE models and wavefront control algorithms in our day-to-day activities, with PROPER serving as an independent cross-check for final validations.

4.4 System Testing

This demonstration will be carried out primarily in JPL’s High Contrast Imaging Testbed vacuum chamber HCIT-2, supported by the Ames Coronagraph Experiment (ACE) testbed. The demonstration will be in a 10% spectral bandpass, centered at 650 nm. The inner working angle will be $2 \lambda/D$ or better, with the details to be determined during the design period of the proposed effort. No fast dynamic perturbations (tip-tilt, etc.) will be deliberately inserted, and the “star” will be a point source (effectively). As such, this demonstration can be considered a static contrast demonstration. However, we will characterize the sensitivity of the system to x,y, and z displacements of the fiber, and compare to the theoretical sensitivity (Section 4.1.2.1), following the process that was used for WFIRST testing (which will inform how tolerant the system is to different levels of low order errors). We now describe the capabilities and our technical approach on both facilities.

4.4.1 Description of HCIT-2 and past performance with PIAA and PIAACMC

The WFIRST PIAACMC testbed layout is shown in Fig. 6. We will utilize and remanufacture a very similar system to the one designed and successfully tested during the technology development of the WFIRST PIAACMC coronagraph testing at HCIT. This system consists of 2 aspheric mirrors PIAA 1 and PIAA 2 that are arranged as a Gregorian telescope system. The mirrors are mounted on a tube that mechanically connects the primary with the secondary. The secondary mirror is mounted on axis and supported by a spider that mimics the WFIRST telescope spider or any relevant aperture including the secondary obstruction, spiders and any primary mirror segmentation.

The PIAA mirror shapes will be redesigned, but likely fit in a near-identical assembly. The remaining coronagraphic components (pupil stop, occulting mask, Lyot stop, field stops) will also be updated, but there will be no fundamental changes from the WFIRST PIAACMC layout to accommodate this effort.

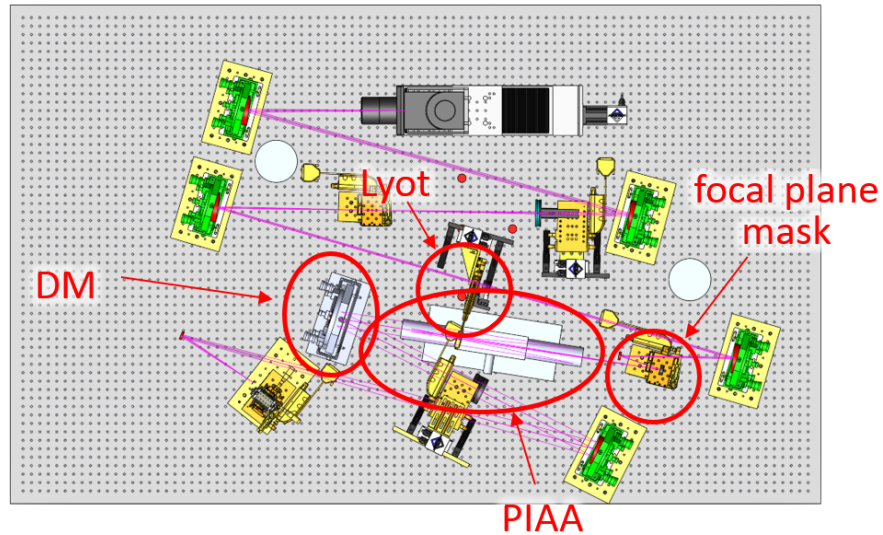
One of the most critical parameters for our testing is testbed jitter. In May of 2016, measurements of testbed jitter were performed on the PIAACMC coronagraph at HCIT-2 under vacuum. These measurements were based on a sequence of PSF images taken at 400Hz, 50 μ s exposures, over a time interval of \sim 1000s. The resulting total level of jitter was 0.002 λ/D rms per axis. For this program, we conservatively assume the testbed jitter to be 0.004 λ/D , and are adopting a baseline jitter tolerance requirement of 0.008 λ/D jitter for coronagraph design.

4.4.2 HCIT-2 proposed testing

The technical approach adopted here to achieve the static contrast milestone is based on the successful practices employed during previous TDEMs and in the WFIRST coronagraph technology development efforts. HCIT has staff uniquely experienced and qualified for this type of work. Institutional PI Kern (with Guyon) previously ran the TDEM09 PIAA and TDEM10 PIAA efforts on HCIT (Guyon et al. 2014a, Guyon et al. 2014b), and played a key role in HCIT demonstrations for TPF-C milestone 1 (Trauger et al. 2006), TPF-C milestone 2 (Kern et al. 2008) and TDEM09 VVC (Serabyn et al. 2014). Kern also played key roles on TDEM09 wavefront sensing (Noecker et al. 2012) and TDEM10 model validation (Shaklan et al. 2015) experiments. Kern has also been a key member of all three WFIRST coronagraph testbed teams, leading the PIAACMC team (Kern et al. 2016).

The PIAACMC design for the SCDA study will be re-optimized for a simpler testbed layout, involving mild changes to the mirror shapes and occulting mask. The tools used for this optimization will be based on the ones used for the SCDA and WFIRST designs, which are in turn

the same tools used for the WFIRST design. This design phase will produce mirror shapes and occulting mask designs for fabrication, as well as CGH designs for testing the mirror shapes. The optimization tools will consider a 10% bandpass, as well as the reduction in tip-tilt sensitivity needed to produce good contrast in the presence of finite stellar angular diameter, appropriate to the angular resolution of a LUVOIR segmented aperture.



NOTE: DRAWING NOT TO SCALE

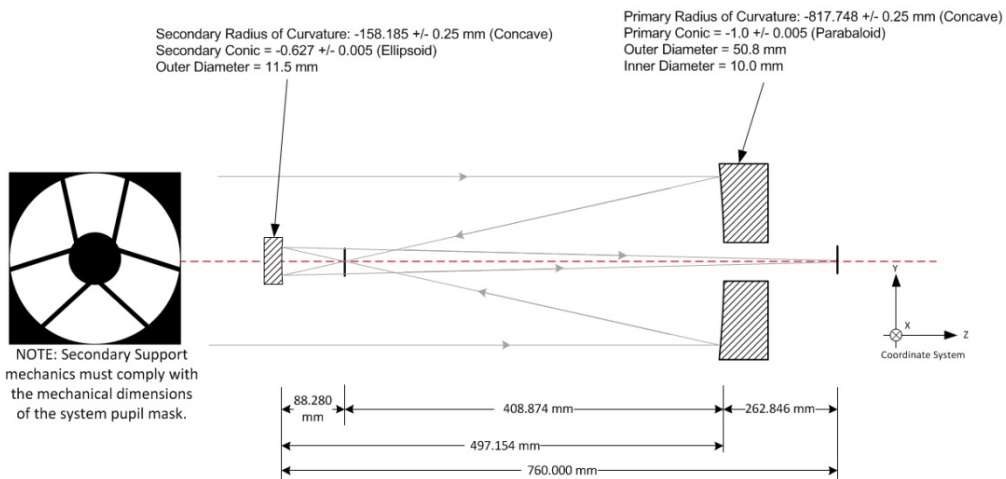


Figure 6. Top: Optical layout of WFIRST PIAACMC testbed. Bottom: PIAA mirror geometry for the WFIRST PIAACMC design. The details of our design for both layouts may differ, but overall will be schematically similar.

Once the testbed has been upgraded to a segmented PIAACMC design, the wavefront control demonstration begins. This follows a style of investigation performed in many contexts previously

on HCIT. If the past is any guide, there will likely be several intermediate limitations to contrast that will have to be overcome, involving such issues as registration of stops, ghosts, testbed vibrations, DM electronic stability, fiber optic polarization, etc. It should be expected that as the system is better understood during these tests, adjustments will be made to either the test hardware, the wavefront control software, or the PIAACMC design.

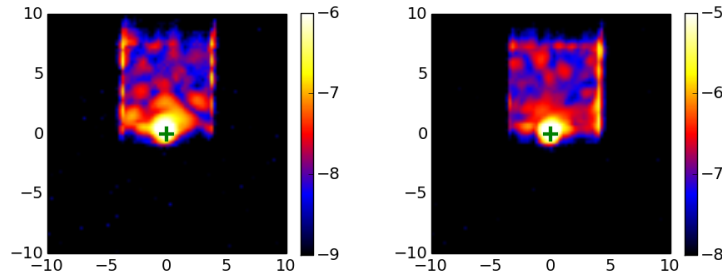


Figure 7. WFIRST PIAACMC results: (left) monochromatic contrast of $2.6e-8$; (right) broadband contrast of $1.8e-7$.

The schedule assumes that each test cycle of this experiment will receive a 2-month testing period followed by 2 months idle, as HCIT is a shared facility and an unknown list of other projects will schedule their time. The two months of testing will be a sequence of calibration, EFC wavefront control (Give'on et al. 2007) to see improved contrast, and diagnostic tests of different performance aspects. These diagnostic tests typically involve measurements of sensitivities, and often spatial / temporal / spectral / polarization decomposition of existing dark hole speckle morphologies to identify likely matches or mismatches with respect to expectations based on propagation models. The two months spent with the testbed idle will be a chance to further analyze the data and performance metrics obtained, integrate the products from continued mask fabrication and characterization, make structural changes to the wavefront control algorithms, and plan the following experimental run. This is typical of all past HCIT experiences, and the HCIT staff have accumulated a significant body of diagnostic tools and algorithmic options over the last 14 years.

4.4.3 ACE testing

The coronagraph at the Ames Coronagraph Experiment testbed will be used to test the focal plane CMC mask manufactured at the UofA in an end-to-end coronagraph down to $\sim 1e-7$ contrasts to mature it to the point where it is ready for vacuum testing.

The ACE testbed is a state-of-the-art facility operating in temperature-stabilized air, designed for development of coronagraph technologies and focusing on the PIAA coronagraph development. It has been pushing state of the art performance at IWAs $< 2 \lambda/D$ (Figure 8 and e.g. Belikov et al. 2013).

The ACE lab features existing and proven advanced hardware, which will be used for the work in this proposal:

- Fully functioning wavefront control system that includes a 32x32 Boston Micromachines Corporation (BMC) DM with several wavefront control algorithms.
- PIAA coronagraph (Guyon et al. 2011) consisting of PIAA mirrors, occulting mask, as well as inverse PIAA lenses and mirrors.
- Several light sources coupled into single-mode fibers to create star images as if they were delivered by a telescope into our instrument.

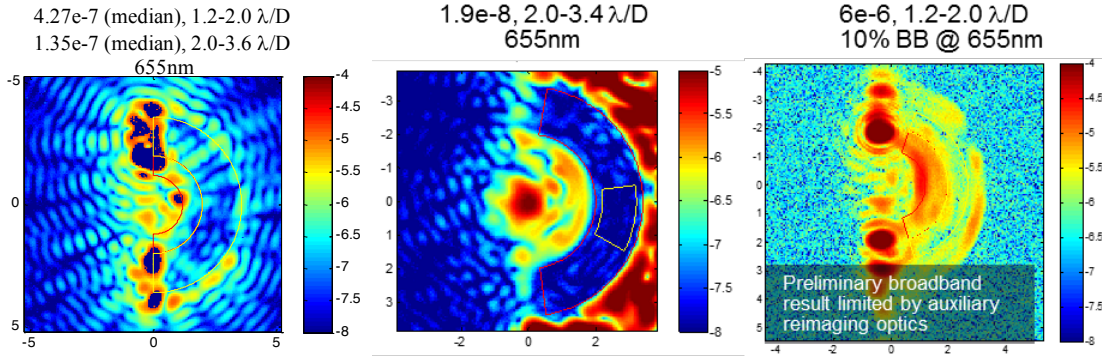


Figure 8. ACE lab high contrast demonstrations, showing, respectively, $4.3\text{e-}7$ and $1.4\text{e-}7$ (median) contrasts in the $1.2\text{-}2.0 \lambda/D$ and $2.0\text{-}3.6 \lambda/D$ regions at 655nm ; $1.9\text{x}10^{-8}$ mean contrast between 2.0 and $3.4 \lambda/D$; and $6\text{e-}6$ contrast between 1.2 and $2.0 \lambda/D$ in a 10% -wide band centered on 655nm (dark zones are shown by red and yellow outlines).

Although evaluating masks at ACE down to $1\text{e-}7$ contrasts does not prove they will be capable of achieving $1\text{e-}9$ at HCIT, it is still important to do the ACE test for several reasons. First, it reduces the potential problems with the mask only to ones that are between $1\text{e-}9$ and $1\text{e-}7$ level. Second, it allows validating models of the UofA mask at least down to $1\text{e-}7$ level, which is an important first step that can be done at lower cost at ACE than HCIT. These models can then be used, in conjunction with measured mask errors, to predict whether they will reach $1\text{e-}9$ contrast at HCIT before testing them. Third, as risk mitigation, we will have a mask wheel during vacuum tests which can switch back to the MDL mask if it becomes apparent early in the test that the UofA mask cannot meet the milestone.

5 Data Measurement & Analysis

This section describes the details of the data measurements and analysis to reach milestones 1-3. Although milestone 1 is based on computer simulations and the other two are lab demonstrations, we are keeping our analysis and data products as similar as possible between different milestones, regardless of whether the data comes from a computer or the lab. This helps keep the simulations as relevant as possible to the lab demonstrations, allows calibrating our testbed models better, and enables testing and debugging our analysis methods on simulated data, which is more efficient. However, some calibrations described below (e.g. star brightness, plate scale) will of course be known a priori for milestone 1 because they would be specified in a configuration file read by the simulator code. These calibrations are labeled as "milestones 2 and 3 only".

5.1 Definitions

The contrast metric requires a measurement of the intensity of speckles appearing within the dark field, relative to the intensity of the incident star. In the following paragraphs we define the terms involved in this process, spell out the measurement steps, and specify the data products.

The definitions below are based on standard ones established in many previous TDEM projects, but it should be noted that a recent study by a Study Analysis Group of the ExoPAG (Jensen-Clem et al. 2017) proposed new definitions and a figure of merit called the "performance

gap", which is based on fundamental concepts in signal detection theory. In order to maintain continuity with past projects, we will continue using the older established definitions for purposes of formalizing milestones and success criteria, but also explore the "performance gap" metric as time permits.

5.1.1 "Raw" Image and "Calibrated" Image (milestones 2 and 3 only)

Standard techniques for the acquisition of camera images are used. We define a "raw" image to be the 2D array of pixel values image obtained by reading the charge from each pixel of the camera detector, amplifying and sending it to an analog-to-digital converter. We define a "calibrated" image to be a raw image that has had background bias subtracted and the detector responsivity normalized by dividing by a flat-field image (if the flat field is significantly non-uniform). Saturated images are avoided by choosing appropriate settings for the exposure time, camera gain (if selectable) and source brightness in order to avoid the confusion of camera detector blooming and other potential camera detector nonlinearities. All HCIT-2 raw images are permanently archived and available for later analysis.

5.1.2 DM flat (milestones 2 and 3 only)

We define "flat" to be a DM setting in which actuators are set to a predetermined surface figure that is approximately flat (typically, about 20 volts on each actuator for a Xinetics DM, and ~100V for a BMC DM, with appropriate variations to make the surface figure flat).

5.1.3 Star (milestones 2 and 3 only)

We define the "star" to be either: (a) a bare single mode fiber tip, 0.22 numerical aperture with light relayed via the optical fiber from a source outside the optical enclosure wall (e.g. 650 nm frequency-stabilized laser), or (b) a small pinhole illuminated by a fiber (5 μ m or smaller). This "star" is the only source of light in the optical path. It is a stand-in for the star image that would have been formed by a telescope system in a focal plane immediately upstream of the coronagraph.

5.1.4 Wavefront control iteration.

We define "wavefront control iteration" to be a measurement of the complex-valued field in the dark zone followed by a DM correction aimed at removing coherent light in the dark zone. Such iterations will be repeated for as many cycles as are needed to reach a desired level of speckle suppression.

5.1.5 Contrast field

The "Contrast field" is a dimensionless map (2D array of numbers) representing for each pixel of the detector, the ratio of its value to the value of the peak of the central PSF that would be measured in the same conditions (camera setting, exposure time, central source illumination at the input of the instrument) if the coronagraph focal plane mask were removed. Measurement of the contrast field is detailed in sec. 5.4.

5.1.6 Contrast value

"Contrast value" is a dimensionless quantity which is the average value of the contrast field over the dark zone adopted for the experiment. Its measurement is detailed in sec. 5.5. When

talking about average value of the contrast field over regions other than the dark zone, we use the term "mean contrast".

5.1.7 "Statistical Confidence" (milestones 2 and 3 only).

The measurement of coronagraph instrument contrast at levels better than the success threshold must be statistically significant, ensuring that success is not an artifact of the tails of a noise distribution. This noise, averaged over the dark zone, comprises measurement noise (read noise and shot noise) and systematic noise (photometric calibration).

The measured contrast, averaged over the dark zone, will be considered significantly better than the threshold if it is at least 3σ below the threshold contrast. If the noise were Gaussian, this would correspond to the threshold being outside of a 99.9% one-sided confidence interval about the measured contrast. The σ adopted for this criterion accommodates both the measurement noise averaged over the dark zone and calibration uncertainty. HCIT typically experiences calibration uncertainties on the order of 2-3%, and it is straightforward to take images with measurement noise well below this level. This means that the measured contrast will have satisfied the statistical confidence requirement if the demonstrated contrast value is ~ 6 -10% better than the contrast threshold stated in the milestone.

It should be noted that this definition is a significant simplification of the statistical confidence criterion used in previous HCIT TDEM projects, which relied on 3 sets of data with 1000 measurements each. That criterion was based on repeatability and stability constraints designed to test the environmental and wavefront control properties of the testbed, which are now well established. On the other hand, the experiment described here is designed to isolate the effects of the coronagraphic architecture and elements, and so does not include general testbed verification activities. Also, from experience, experiments that passed the simpler metric presented here have never failed the more complicated criterion used in the past projects.

For a successful high-contrast demonstration, the architecture-specific coronagraphic elements (PIAA mirrors, occulting mask, Lyot stop) must be properly fabricated and aligned, and in addition, the supporting equipment must all be functioning nominally -- this includes the deformable mirror, all motion control stages and actuators, the light source, the testbed thermal and vacuum environment, and all support electronics. The milestone demonstrations can be idealized as attempts to identify the limiting performance allowed by the coronagraphic components, but they are often limited by the performance of the non-coronagraphic elements. Once measurement and systematic noise have been understood and accounted for, no combination of behaviors of the non-coronagraphic elements can produce results better than the limits set by the coronagraphic elements. In this way, the best achieved performance can be interpreted as an upper limit on the ultimate performance allowed by the architecture-specific coronagraphic elements.

5.2 Measurement of the Star Brightness (milestones 2 and 3 only)

All "contrast" measurements are normalized to the intensity peak obtained when the occulter is removed and the Lyot stop is in place (unocculted star peak brightness). Because the camera dynamic range is typically $\sim 10^4$, a so-called "photometric fiducial ladder" calibration procedure is necessary to enable measurements of contrast as low as 10^{-9} . This is done by identifying several fiducial regions in the focal plane, i.e. regions a few λ/D wide consisting of speckles whose shape and contrast does not vary much during wavefront control actuation of the DM. In a typical ladder,

the first fiducial region is the unocculted PSF itself, the second region can be with the occulter in or out, and having contrast of about 10^{-3} , the third region is with the occulter in, and contrast of about 10^{-6} , etc.

Mean contrast of these fiducial calibration regions is measured by induction. Specifically, in the zeroth step, the occulter is moved out and the exposure time (and if possible, laser power) is set such that the unocculted PSF is close to saturation, but still in the linear range of the detector. Thus, contrast of each pixel in the image can be directly computed by normalizing pixel values to the peak brightness of the PSF. Mean contrast in this region 1 (PSF core) is also computed.

Then, during the n -th step, assume that the mean contrast of the n -th region is known. An image is taken with exposure time (and if possible, laser power) set such that n -th and $n+1$ -st regions are both seen unsaturated with high SNR, and within the linear response of the detector. The knowledge of mean contrast in the n -th region then allows computing the contrast of each pixel in that image as well as calibrating the mean contrast in the region $n+1$. This completes the induction and allows measurement of contrast down to any level as long as fiducial regions can be found at every step of the induction.

5.3 Measurement of the focal plane scale

The focal plane scale is defined by the displacement (pixels) of the PSF's photocenter in the absence of a focal plane mask in the system for a physical displacement of the light source by $f\lambda/D$, where f and D are respectively the focal length and diameter of beam at the input of the system (before PIAA optics). All angular separations given in this document adopt this definition. The PSF photocenter is defined as the intensity-weighted center of the PSF, and is a linear function of the source position at the input of the system. With the above definition, the focal plane scale value obtained is independent of the source offset used in the measurement. We will empirically measure the focal plane scale (both in the lab and in the simulator) by moving the light source by a known amplitude and measuring its photocenter, and verify that the obtained scale matches the value expected from the optical design of the PIAA mirrors and re-imaging optics.

5.4 Measurement of the Coronagraph Contrast Field

Each "coronagraph contrast field" (sec. 5.1.5) is obtained as follows:

1. The occulting mask is placed on the star image.
2. A long-exposure (e.g. seconds) image is taken of the coronagraph field (i.e. the suppressed star plus surrounding speckle field) with the coronagraph focal plane mask in place. The dimensions of the dark zone target areas are defined as follows: A dark zone extending from 2 to $8 \lambda/D$, demonstrating a useful search space, is bounded by a line that passes $2 \lambda/D$ from the star at its closest point, and by a circle of radius $8 \lambda/D$ centered on the star (see Figure 9).
3. The resulting image is divided by the peak value of the reference star to produce a "contrast field" image, as discussed in Sec. 5.2.

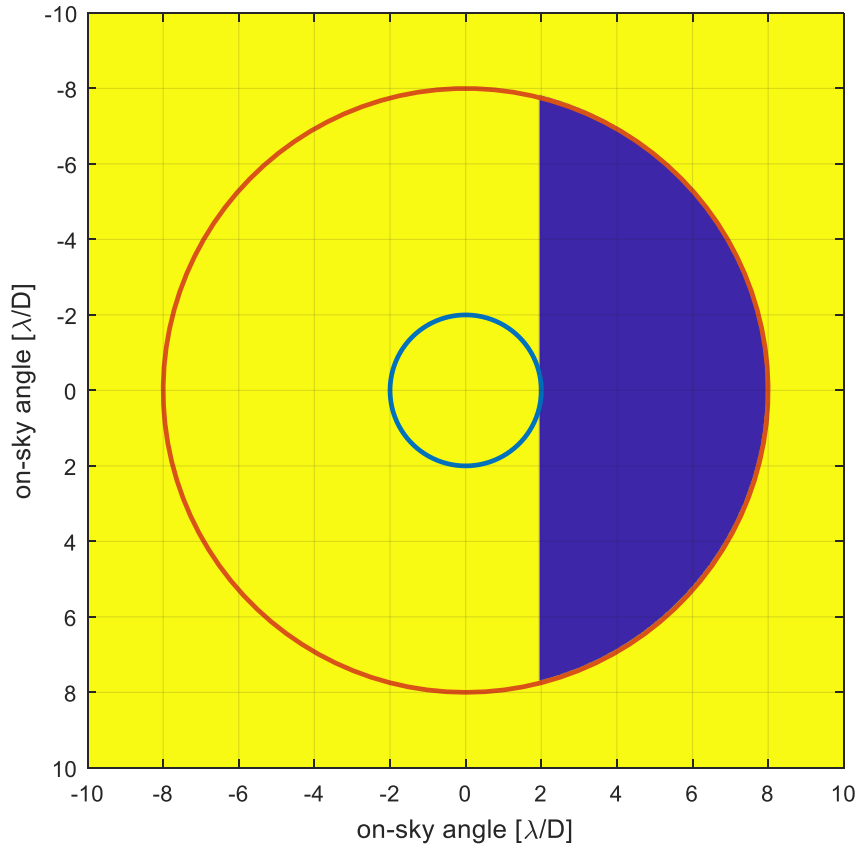


Figure 9. Dark zone geometry. The blue and red circles correspond to the inner and outer working angles, respectively. The D-shaped high contrast region, or "dark zone", is shown in blue.

5.5 Contrast value for a single measurement

The contrast field is averaged within the dark zone (Figure 9) to yield the contrast value (Sec. 5.1.6) for a single measurement. This averaging is done over a single image (which itself may consist of a co-addition of consecutive camera frames) with no statistical filtering other than removal of detector defects such as bad pixels and cosmic rays.

5.6 Milestone Verification Demonstration Procedure

The Milestone validation demonstration procedure is as follows:

1. The DM is set to flat (Sec. 5.1.2) with a reset of the wavefront control system software.
2. Wavefront control iterations are performed to iteratively converge to settings of the DM actuator driver voltages that give an acceptable high-contrast wavefront solution for the target dark zone. This typically takes several hours, starting from flat, if no prior information is available.
3. When contrast in the dark zone stops improving, a typical high-contrast measurement is made. This measurement is referred to as the contrast field image.

4. All images and data required by the certification data package (Sec. 5.7) are saved and archived.

5.7 Milestone Certification Data Package

The Principal Investigator will assemble a milestone certification data package for review by the Exoplanet Exploration Program and its Technology Advisory Committee. In the event of a consensus determination that the success criteria have been met, the Program will submit the findings of the TAC, together with the certification data package, to NASA HQ for official certification of milestone compliance. In the event of a disagreement between the Program and the TAC, NASA HQ will determine whether to accept the data package and certify compliance or request additional work.

The milestone certification data package will contain the following explanations, charts, and data products.

1. A narrative report, including a discussion of how each element of the milestone was met, an explanation of each image or group of images, appropriate tables and summary charts, and a narrative summary of the overall milestone achievement.
2. Calibrated images of the coronagraph transmittance profile.
3. Calibrated images of the data set, with appropriate numerical or color-coded or greyscale coded contrast values indicated, and with coordinate scales indicated in units of Airy distance (λ/D), all in demonstration of achieving the milestone elements.
4. A histogram of the brightness distribution of pixels in the high contrast dark field.
5. A set of contrast measurement values.
6. A description of the residual components of the residual light in the dark zone: static coherent light, dynamic coherent light (due to time-variable pointing errors and wavefront changes too rapid to be fully corrected by the wavefront control loop) and incoherent light (ghosts, polarization leaks).
7. A plot of contrast vs. EFC iteration, as well as a plot showing contrast stability vs. time. This plot will have enough iterations to illustrate the statistical behavior of contrast during EFC operation as well as after it converged.
8. A step-by-step description of all data processing and analysis performed, along with source code and algorithm description. This will be provided in sufficient detail so an independent analysis of the raw data can be applied outside our team.

6 Success Criterion

Milestones 1, 2, and 3 are to be considered successfully met if the conditions specified by milestones 1, 2, and 3 (Sec. 3) are satisfied, with sufficient statistical confidence as described in Sec. 5.1.7.

7 Schedule

This effort spans three years and is diagrammed at a high level in Figure 10. The green path is a "primary" path which uses a CMC mask made by MDL, with both the mask style and process that was proven in the WFIRST program. Because the CMC mask carries the highest risk, our plan also includes an alternative CMC development and testing path, with dotted lines indicating points at which it can be inserted into the primary testing path if it is determined to be more likely to succeed than the MDL mask.

Our efforts will start with 5 months of coronagraph design led by Bryson (with Guyon, Belikov, Kern, and Knight) using the methods described in section 1.4, using pupils used by LUVOIR and HabEx as working versions as of Dec 2017. PIAA mirrors, CMC mask, and Lyot stops will all be designed to meet milestone 1, and each design iteration is verified through two independent wavefront control simulations by Dan Sirbu and Brian Kern. The design trade space will be explored and a design selected that has the least sensitivity to aberrations, including those arising from polarization effects, while meeting the milestones in simulation.

At the completion of the coronagraph design task, a vendor-readable specification for the PIAA mirrors will be generated and delivered to the coronagraph fabrication task as well as the vacuum testbed layout task. The mirrors, stops, and masks will then be fabricated. The mirrors are the longest-lead items, requiring 3 months for fabrication (based on WFIRST experience). Accompanying the mirror order is a set of JPL-provided CGHs for optical testing. The mirror and stop fabrication will be accomplished through purchase orders during this period. Two sets of mirrors will be fabricated, both to reduce schedule delays in case one set is damaged, as well as to enable the testing of the alternative CMC mask at the ACE testbed. The second set is lower cost than the first because it can reuse the CGH and several other aspects of PIAA manufacturing.

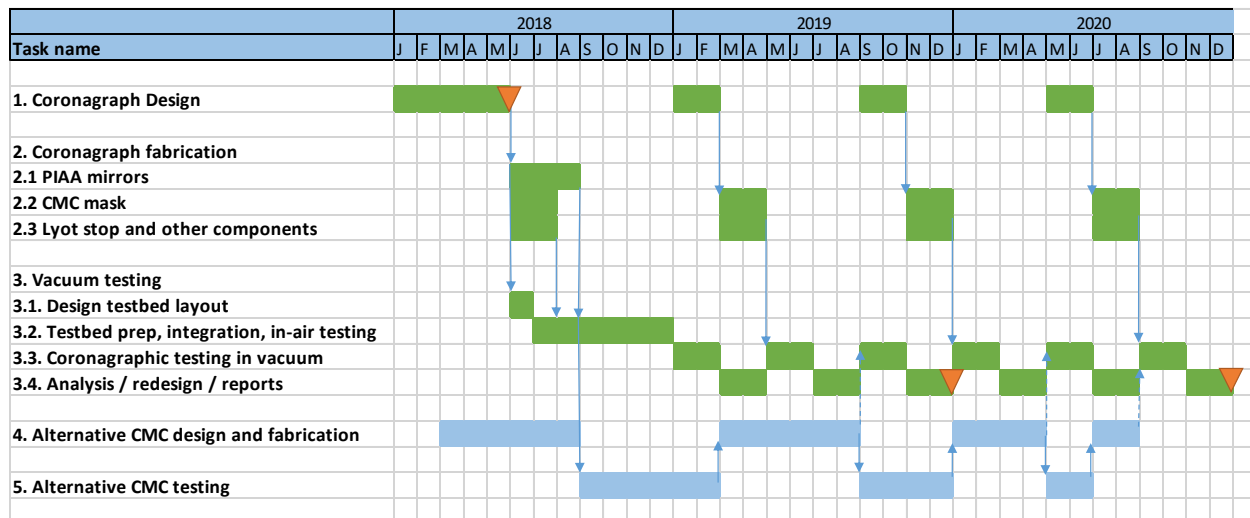


Figure 10. High-level schedule. Green represents the primary path that assumes the baseline CMC mask made by MDL and blue represents a path to develop and test an alternative mask, which reduces risks on the baseline CMC mask as well as enables a potentially more powerful mask. Dotted lines represent backup options in case the alternative mask is determined to be more likely to meet the milestones. Milestones are represented by orange triangles

The mask fabrication will be done at JPL's MDL by Wilson assisted by an MDL technician, and will take place concurrently with the mirror fabrication. Two cycles of mask fabrication will be performed during this period, allowing for a cycle of mask fabrication, followed by detailed characterization, and feedback of mask errors to a second round of fabrication and characterization. This two-cycle feedback pattern will be repeated three more times through the entire effort, each time producing one fabrication and characterization per month (at a fractional effort).

In addition to the CMC mask, other coronagraph and auxiliary components will be fabricated, including the Lyot stop and the segmented entrance pupil masks.

Concurrently with the coronagraph component fabrication, the HCIT2 testbed layout will be designed over one month, led by Bendek (with Kern), followed by HCIT2 preparation, and integration led by Wilson. While coronagraph components are being fabricated, all required non-coronagraphic components and electronics will be gathered, installed, and tested. As coronagraphic components arrive, they will also be verified, installed, and aligned. After the alignment is complete, initial tests and calibrations will be conducted in air to make sure the system performs as expected, at least down to mild contrasts that are possible in air. Based on experience, a new high contrast imaging system usually requires a testing and debugging period of several months prior to moving into vacuum. These tests will include characterizations of tip/tilt jitter.

With the in-air tests complete, the testbed will execute 6 cycles consisting of 2 months of vacuum testing, followed by a 2-month period of analysis / redesign following the methods described in section 4.4. One of the earliest measurements we will perform in vacuum is the verification that testbed jitter is $< 0.004 \lambda/D$ rms per axis. Sirbu, Kern, and Marx will be performing wavefront control and supporting modeling tasks during the vacuum testing periods, and the design team (Bryson / Guyon / Belikov / Kern / Knight) and fab team (Wilson) will produce an improved mask for the even-numbered cycles (#2, 4, and 6). Cycles 3, 5, and 6 can receive the alternative CMC mask made by UofA, with a decision on that being made based on the performance of the MDL mask as described in the following paragraph.

Concurrent with the primary CMC effort (green), the alternative CMC mask effort (blue) will consist of cycles of CMC mask fabrication and testing at the ACE testbed to raise its TRL sufficiently for vacuum tests. The mask design and fabrication effort will be led by Guyon and Knight. The early design and test cycles will start out longer to accommodate early development and infrastructure, but as the technology of that mask matures, cycles will accelerate. The first design cycle will take 6 months (starting 2 months after project start). At start of month 8 of year 1, the ACE testbed will receive the 2nd copy of the PIAA mirrors and masks, and the alternative CMC mask, and commence integration, alignment, and testing, led by Belikov (with Sirbu, Pluzhnik, and Bendek), which will take 6 months. The results of those tests will expose any limiting factors due to the mask and inform a second design iteration of the mask in year 2 by UofA. Any lessons learned from HCIT2 testing will also serve to inform this design. Once the mask is completed in month 8 of year 2, a decision will be made about whether cycle 3 of HCIT testing will proceed with the MDL or UofA mask for the final milestone 1 test. This decision will be based on the performance of the MDL mask and the maturity of the UofA mask from ACE tests. In either case, a copy of the UofA mask will be tested at ACE in year 2. Similarly, there will be a third design and test cycle in year 3, followed by a final 4th iteration design of the UofA mask. This sequence is designed such that the final two HCIT2 tests in year 3 will have the option of using either the MDL or UofA mask for the final milestone at the end of year 3.

8 References and Citations

- Belikov, R., Bendek, E., Greene, T.P., Guyon, O., Lozi, J., Lynch, D. H., Newman, K. E., Pluzhnik, E., Schneider, G., Tenerelli, D., Thomas, S.J., Witteborn, F. C., "EXCEDE Technology Development II: Demonstration of High Contrast at 1.2 I/D and preliminary broadband results," *Proc SPIE* 8864-31 (2013).
- Give'on, A., Kern, B., Shaklan, S., Moody, D.C., Pueyo, L. 2007, "Broadband wavefront correction algorithm for high-contrast imaging systems," *Proc. SPIE* **6691**, 66910A.
- Guyon, O., Martinache, F., Belikov, R., Soummer, R., "High performance PIAA coronagraphy with complex amplitude focal plane masks," *ApJS* **190**, 2, pp. 220-232 (2010).
- Guyon, O., Kern, B. Belikov, R., Shaklan, S., Kuhnert, A., Give'on, A., "Phase-Induced Amplitude Apodization (PIAA) coronagraphy: recent results and future prospects," *Proc SPIE* 8151 (2011).
- Guyon, O., Kern, B., Kuhnert, A. 2014a, "Phase-Induced Amplitude Apodization (PIAA) Technology Development, Milestone 1: Monochromatic Contrast Demonstration," <http://exep.jpl.nasa.gov/files/exep/PIAAMilestone1.pdf>
- Guyon, O., Kern, B., Kuhnert, A. 2014b, "Phase-Induced Amplitude Apodization (PIAA) Technology Development, Milestone 3: 10% Bandpass Contrast Demonstration," <http://exep.jpl.nasa.gov/technology/Guyon-PIAA-Milestone-3.pdf>
- Guyon, O., Hinz, P.M., Cady, E., Belikov, R., Martinache, F. 2014c, "High Performance Lyot and PIAA Coronagraphy for Arbitrarily Shaped Telescope Apertures," *ApJ* **780**, 171.
- Jensen-Clem, R., Mawet, D., Gomez Gonzalez, C.A., Absil, O., Belikov, R., Currie, T., Kenworthy, M.A., Marois, C., Mazoyer, J., Ruane, G., Tanner, A., "A New Standard for Assessing the Performance of High Contrast Imaging Systems," *accepted by ApJ* (2017).
- Kern, B., Kuhnert, A., Trauger, J. 2008, "Exoplanet Exploration Coronagraph Technology: Technology Milestone #2 Report," <http://exep.jpl.nasa.gov/TPF-C/HCIT-Milestone2Signed-2008-08-08.pdf>
- Kern, B. et al. 2016, "Phase-induced amplitude apodization complex mask coronagraph mask fabrication, characterization, and modeling for WFIRST-AFTA," *J. Astron Telesc. Instrum. Syst.* **2**(1), 011014.
- Knight, M. J., Brewer, J., Hamilton, R., Ward, K., Milster, T.D., Guyon, O., "Design, fabrication, and testing of stellar coronagraphs for exoplanet imaging," *Proc. SPIE* **10400** (2017).
- Krist, J. 2014, "End-to-end numerical modeling of AFTA coronagraphs," *Proc. SPIE* **9143**, 91430V.
- Krist, J., Nemati, B., Mennesson, B. 2015, "Numerical modeling of the proposed WFIRST-AFTA coronagraphs and their predicted performances," *J. Astron Telesc. Instrum. Syst.* **2**(1), 011003.
- N'Diaye, M. et al. 2016, "Apodized Pupil Lyot Coronagraphs for Arbitrary Apertures. V. Hybrid Shaped Pupil Designs for Imaging Earth-like Planets with Future Space Observatories," *ApJ* **818**, 163.

- Newman, K., Guyon, O., Balasubramanian, K., Belikov, R., Jovanovic, N., Martinache, F., Wilson, D., “An Achromatic Focal Plane Mask for High-Performance Broadband Coronagraphy,” *PASP* 127, Iss 951, pp. 437-444, (2015).
- Noecker, C. et al. 2012, “Advanced Speckle Sensing for Internal Coronagraphs,” http://exep.jpl.nasa.gov/files/exep/Speckle%20Sensing%20TDEM%20Final%20Report_v12.pdf
- Serabyn, E. et al. 2014, “Technology Milestone #1 Report : Vortex Coronagraph Technology,” http://exep.jpl.nasa.gov/technology/Serabyn_Final_2010.pdf
- Shaklan, S. et al. 2015, “Technology Milestone #1A Final Report: Coronagraph Starlight Suppression Model Validation,” https://exep.jpl.nasa.gov/files/exep/COMBINEDv5_Milestone%203A%20Final%20Report%20072915.pdf
- Stark, C.C. et al. 2015, “Lower Limits on Aperture Size for an ExoEarth Detecting Coronagraphic Mission,” *ApJ* **808**, 149.
- Trauger, J., Kern, B., Kuhnert, A. 2006, “TPF-C Technology Milestone #1 Report,” http://exep.jpl.nasa.gov/TPF-C/TPFC_M1_Report_060710_final.pdf
- WFIRST milestone 3 report:
https://wfirst.gsfc.nasa.gov/science/sdt_public/wps/references/WFIRST_CGI_Milestone3_Final_Report.pdf

9 **List of Acronyms**

ACE	Ames Coronagraph Experiment laboratory
AFM	Atomic Force Microscope
APLC	Apodized Pupil Lyot Coronagraph
ARC	Ames Research Center
BMC	Boston Micromachines Corporation
CGH	Computer-Generated Holograph
CMC	Complex-valued Mask Coronagraph
Co-I	Co-Investigator
DM	Deformable Mirror
EFC	Electric Field Conjugation
ELT	Extremely Large Telescope
E-ELT	European Extremely Large Telescope
ExoPAG	Exoplanet Program Analysis Group
FPM	Focal Plane Mask
HabEx	Habitable Exoplanet Imaging Mission
HCIT	High Contrast Imaging Testbed
HQ	Headquarters
IWA	Inner Working Angle
JPL	Jet Propulsion Laboratory
LUVOIR	Large UltraViolet / Optical / InfraRed Surveyor
MDL	MicroDevices Laboratory
NASA	National Aeronautics and Space Administration
PI	Principal Investigator
PIAA	Phase Induced Amplitude Apodization
PIAACMC	PIAA Complex-valued Mask Coronagraph
PROPER	An optical propagation library
PSF	Point Spread Function
SCDA	Segmented Coronagraph Design & Analysis
SCExAO	Subaru Coronagraphic Extreme Adaptive Optics
SNR	Signal to Noise Ratio
SPC	Shaped Pupil Coronagraph
STDT	Science and Technology Definition Team
TAC	Technology Assessment Committee
TDEM	Technology Development for Exoplanet Missions
TPF-C	Terrestrial Planet Finder - Coronagraph
UofA	The University of Arizona
VVC	Vector Vortex Coronagraph
WFIRST	Wide Field InfraRed Survey Telescope